RSC Advances




ROYAL SOCIETY OF CHEMISTRY

www.rsc.org/advances

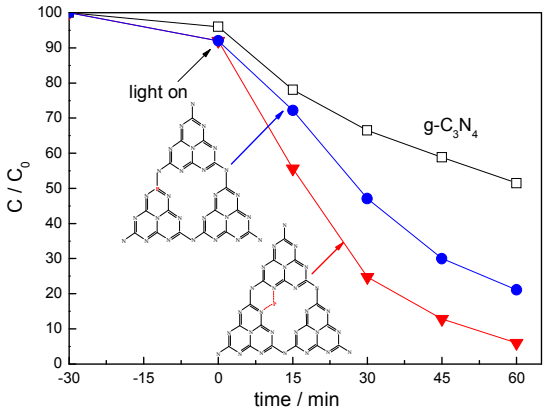


Interstitial P doping is more effective to improve the photocatalytic activity compared with substitutional P doping.

Cite this: DOI: 10.1039/c0xx00000x

www.rsc.org/xxxxxx

ARTICLE TYPE

# A simple and efficient method to prepare phosphorus modified g-$C_3N_4$ visible light photocatalyst

**Shaozheng Hu,*[a] Lin Ma,[b] Jiguang You,[c] Fayun Li,[a] Zhiping Fan,[a] Fei Wang,[c] Dan Liu[d] and Jianzhou Gui*[d]**

***Received (in XXX, XXX) Xth XXXXXXXXX 20XX, Accepted Xth XXXXXXXXX 20XX***
**DOI: 10.1039/b000000x**

Phosphorus doped g-$C_3N_4$ was prepared by a simple method using dicyandiamide monomer and diammonium hydrogen phosphate as precursors. X-ray diffraction (XRD), UV-Vis spectroscopy, Fourier transform infrared spectra (FT-IR), photoluminescence (PL), X-ray photoelectron spectroscopy (XPS) and photocurrent measurement were used to characterize the prepared catalysts. The results indicated that the introduction of phosphorus inhibited the crystal growth of graphitic carbon nitride, decreased the band gap energy and increased the separation efficiency of photogenerated electrons and holes. P doping site is influenced by the phosphorus source. Interstitial P doping is more effective to improve the photocatalytic activity of Rhodamine B (RhB) degradation compared with substitutional P doping. The possible mechanism was proposed.

## Introduction

Photocatalytic oxidation of aqueous organic pollutants into $CO_2$, water and other nonhazardous compounds is one of the environmentally friendly manners to remove the organic pollutants in water.[1] One of the primary challenges in practical application of this technique is to design a robust, cheap and stable photocatalyst that exhibits excellent visible-light absorption as well as efficient separation and transportation of the photogenerated holes and electrons. However, the wide band gap energy and low quantum efficiency are still the "bottleneck" of this technology to meet the requirement of practical application. In the past decades, $TiO_2$ is the most common used photocatalyst. However, $TiO_2$ performs rather poorly in the processes associated with solar photocatalysis because of its wide band gap.[2] For this purpose, the modified $TiO_2$ and $TiO_2$-based nanocomposite photocatalysts have been developed to improve the visible light absorption ability and promote the separation of holes and electrons pairs.[3-9] N doping into $TiO_2$ has been reported to be one of the most effective approaches to enhance the visible light activity.[3] However, Chen et al.[10] and Hu et al.[11] reported that the photocatalytic activity of N doped $TiO_2$ was not stable. The lattice-nitrogen was oxidized easily by photogenerated holes during the degradation reaction, leading to the decrease of activity. Therefore, it is still highly desirable to develop new photocatalyst with enhanced activity under visible light.

Recently, graphitic carbon nitride (g-$C_3N_4$) has attracted a great deal of interest in photocatalytic applications. Carbon nitride can exist in five phases, α, β, cubic, graphitic and pseudocubic, among which graphitic phase is regarded as the most stable structure. The heptazine ring structure and high condensation degree make it possess many advantages, such as good chemical stability, appropriate band gap energy and unique electronic structure. In addition, g-$C_3N_4$ is metal-free and easily-synthesized via one-step polymerization of cheap raw materials. All of these make g-$C_3N_4$ to be the best candidate for photocatalytic application. However, g-$C_3N_4$ also suffers from many disadvantages, such as the low carrier mobility, low visible-light utilization efficiency, high recombination rate and small BET surface area. Therefore, modification of g-$C_3N_4$ with other metal or non-metal element was developed in recent years.[12-18]

It is known that g-$C_3N_4$ contains nitrogen triangles having six lone-pair electrons, which are available for nonmetal doping. Therefore, nonmetal doping of g-$C_3N_4$ seems to be a feasible way to deal with those drawbacks. Yan et al. prepared Boron-doped g-$C_3N_4$ by heating the mixture of melamine and boron oxide.[12] They suggested that boron doping increased the photocatalytic activity of RhB degradation due to the improvement of dye adsorption and light absorption of catalyst. Zhang et al. used elemental sulfur ($S_8$) as the solvent and mediator to promote the photocatalytic performance of prepared g-$C_3N_4$.[13] This sulfur-flux-mediated polymerization route of carbon nitride improved its intrinsic texture, morphology, optical and electronic properties, thus increased the photocatalytic water reduction performance. Generally speaking, conjugated polymer doped with higher periodic elements tends to show narrower band gap. For example, polythiophene shows a decreased band gap than that of polypyrrole.[19] Therefore, phosphorus atom is expected to be the ideal dopant to tune the texture and electronic structure of g-$C_3N_4$. Zhang et al. first synthesized phosphorus doped g-$C_3N_4$ using dicyandiamide and ionic liquid [Bmim]$PF_6$ as raw material.[14] They found the electrical conductivity and photocurrent were significantly improved after phosphorus

doping. After that, Zhang et al. synthesized the phosphorus doped g-$C_3N_4$ using the same raw material.[15] The obtained phosphorus doped g-$C_3N_4$ exhibited obvious improved photocatalytic activities for RhB and methyl orange degradation under visible light. However, ionic liquid [Bmim]$PF_6$ is not an optimal phosphorus source because of its high price and complicated synthesis process. It is known that the doping site can significantly influence the properties of prepared catalysts. There are many literatures concerning the effect of N doping site on properties and photocatalytic performance of prepared $TiO_2$ based catalysts. N dopant can enter the $TiO_2$ matrix by either direct substitution of an oxygen site or by stationing itself interstitially. The difference in doping site could cause the different oxygen vacancy content and band gap structure, thus leading to the difference in activity. Although many metal and non-metal element doped g-$C_3N_4$ catalysts were reported, few of those literatures investigated the effect of doping site on the photocatalytic activity of prepared g-$C_3N_4$ based catalysts. Hence, in this work, a simple method to synthesize phosphorus doped g-$C_3N_4$ using diammonium hydrogen phosphate as phosphorus source is reported. The photocatalytic activities were evaluated in the photocatalytic degradation of RhB under visible light. For comparison, [Bmim]$PF_6$ was also used as the phosphorus source to investigate the effect of P doping site on the structural property, optical property and photocatalytic performance of prepared g-$C_3N_4$ based catalysts. The possible reaction mechanism is proposed.

## Experimental

### Preparation and characterization

In a typical experiment, 3 g dicyandiamide was dissolved into 15 ml deionized water under stirring. Then desired amount of $(NH_4)_2HPO_4$ was added. The obtained solution was heated to 100 $^oC$ under stirring to remove the water. The solid product was dry at 100 $^oC$ in oven, followed by milling and annealing at 520 $^oC$ for 2 h (at a rate of 5 $^oC \cdot min^{-1}$). The prepared catalyst was denoted as P(x%)-CN, where x% stands for the mass percent of $(NH_4)_2HPO_4$ to dicyandiamide. For comparison, g-$C_3N_4$ was prepared following the same procedure as in the synthesis of P(x%)-CN but in the absence of $(NH_4)_2HPO_4$. When ionic liquid [Bmim]$PF_6$ was used to replace $(NH_4)_2HPO_4$ (with the same P quality as $(NH_4)_2HPO_4$) following the same procedure as in the synthesis of P(6%)-CN, the product is denoted as IL-P(6%)-CN.

XRD patterns of the prepared $TiO_2$ samples were recorded on a Rigaku D/max-2400 instrument using Cu-Kα radiation ($\lambda$ = 1.54 Å). UV-vis spectroscopy measurement was carried out on a JASCO V-550 model UV-vis spectrophotometer, using $BaSO_4$ as the reflectance sample. Fourier transform infrared spectra (FT-IR) were obtained on a Nicolet 20DXB FT-IR spectrometer. Elemental analysis was performed with a vario EL cube from Elementar Analysensysteme GmbH. XPS measurements were conducted on a Thermo Escalab 250 XPS system with Al Kα radiation as the exciting source. The binding energies were calibrated by referencing the C 1s peak (284.6 eV) to reduce the sample charge effect. Photoluminescence (PL) spectra were measured at room temperature with a fluorospectrophotometer (FP-6300) using a Xe lamp as excitation source. Working electrodes were prepared as follows: 0.3 g of sample was ground with 0.7 g of ethanol to make a slurry, then coated on an indium-tin oxide glass by the doctor blade method. Photocurrents were measured by electrochemical analyzer (CHI 618C Instruments) in a standard three electrode system which the prepared sample film was used as the working electrodes, a Pt flake as the counter electrode, and Ag/AgCl as the reference electrode. A 500 W Xe-lamp was used to irradiate the working electrode from the back side. A 1.0 M $Na_2SO_4$ solution was used as the electrolyte.

### Photocatalytic Reaction

RhB was selected as model compound to evaluate the photocatalytic performance of the prepared g-$C_3N_4$ based catalysts in an aqueous solution under visible light irradiation. 0.05 g catalyst was dispersed in 200 ml aqueous solution of RhB (10 ppm) in an ultrasound generator for 10 min. The suspension was transferred into a self-designed glass reactor, and stirred for 30 min in darkness to achieve the adsorption equilibrium. In the photoreaction under visible light irradiation, the suspension was exposed to a 250 W high-pressure sodium lamp with main emission in the range of 400-800 nm, and air was bubbled at 130 ml/min through the solution. The UV light portion of sodium lamp was filtered by 0.5 M $NaNO_2$ solution. All runs were conducted at ambient pressure and 30 °C. At given time intervals, 4 ml suspension was taken and immediately centrifuged to separate the liquid samples from the solid catalyst. The concentrations of RhB before and after reaction were measured by means of a UV-Vis spectrophotometer at a wavelength of 550 nm.

## Results and discussion

XRD analysis is used to investigate the phase structure of prepared photocatalysts. The typical (0 0 2) interlayer-stacking peak at 27.3$^o$ corresponds to an interlayer distance of d = 0.32 nm for g-$C_3N_4$, while the peak at 13.1$^o$ represents in-plane structural packing motif (1 0 0) with a period of 0.675 nm.[20,21] No peak for phosphorus species was observed in all the phosphorus-doped g-$C_3N_4$ materials. It is noted that the P(x%)-CN showed an obviously decreased peak intensities with increasing the phosphorus content, indicating that the crystal growth of graphitic carbon nitride is inhibited by introduction of phosphorus. This phenomenon is consistent with previous results.[15,16,22] Besides, compared with g-$C_3N_4$, a slight shift toward a higher 2θ value is observed for IL-P(6%)-CN but not in the patterns of P(x%)-CN catalysts. This is probably due to the different P doping site caused by the different P sources. Because of the radius difference, the lattice distortion of IL-P(6%)-CN should occur when the substitutional doping happen. In the case of P(x%)-CN, P is probably doped into interstitial site which exhibited no influence on the crystal lattice of g-$C_3N_4$.

To characterize the specific surface area of g-$C_3N_4$ based catalysts, the nitrogen adsorption and desorption isotherms were measured (Fig. 2). The isotherm of both g-$C_3N_4$ and P(6%)-CN are of classical type IV, suggesting the presence of mesopores. The hysteresis loop in the low pressure range ($0.4<P/P_0<0.8$) is associated with the intra-aggregated pores. The high-pressure hysteresis loop ($0.8<P/P_0<1$) is related to the larger pores formed by the accumulation of secondary particles. The BET specific

surface areas ($S_{BET}$) of g-$C_3N_4$, P(2%)-CN, P(4%)-CN, P(6%)-CN, P(8%)-CN, P(10%)-CN and IL-P(6%)-CN are calculated to be 10.9, 12.4, 14.8, 16.5, 17.7, 18.6 and 16.9 $m^2 \cdot g^{-1}$. P(6%)-CN and IL-P(6%)-CN exhibit the comparable BET specific surface area. The $S_{BET}$ increases with increasing the P content. This increased $S_{BET}$ could be probably due to that P doping inhibited the crystal growth of graphitic carbon nitride, leading to the formation of more secondary particles. The large $S_{BET}$ can promote adsorption, desorption and diffusion of reactants and products, which is favorable to the photocatalytic performance.

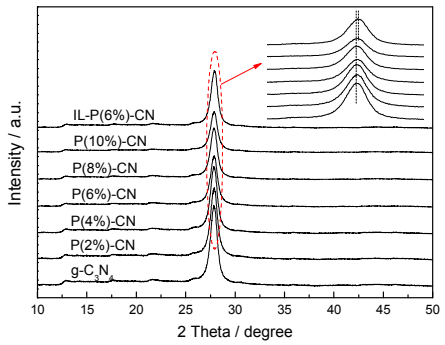


**Fig. 1** XRD patterns of synthesized g-$C_3N_4$, P(x%)-CN and IL-P(6%)-CN.

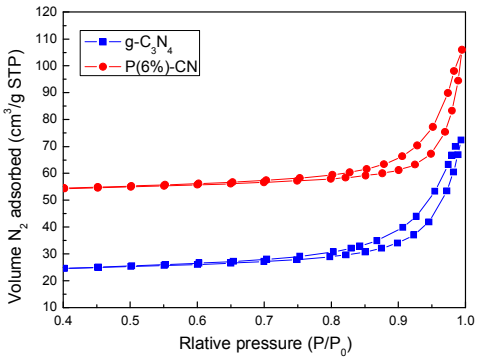


**Fig. 2** $N_2$ adsorption-desorption isotherm of g-$C_3N_4$ and P(6%)-CN.

FT-IR spectra shown in Fig. 3 can provide plentiful structural information concerning of synthesized g-$C_3N_4$, P(6%)-CN and IL-P(6%)-CN. For g-$C_3N_4$, a series of peaks in the range from 1200 to 1600 $cm^{-1}$ are attributed to the typical stretching modes of CN heterocycles, while the sharp peak located at 810 $cm^{-1}$ is assigned to the bending vibration of heptazine rings, which indicating the synthesized g-$C_3N_4$ is composed of heptazine units. The broad absorption band around 3200 $cm^{-1}$ is originated from the stretching vibration of N-H bond, associated with uncondensed aminogroups.[12] For P(6%)-CN and IL-P(6%)-CN, all the characteristic vibrational peaks of g-$C_3N_4$ are observed, suggesting that the structure of g-$C_3N_4$ is not changed after phosphorus doping. Zhang et al.[15] synthesized P doped g-$C_3N_4$ using [Bmim]$PF_6$ as phosphorus source. The vibrations of P-related group were not observed in their investigation. They attributed it to the low phosphorus content or its vibration was overlapped by that of C-N bond. In this investigation, no P-related group was observed in IL-P(6%)-CN, which is consistent with the previous results.[14,15] However, a peak centered at ca. 950 $cm^{-1}$ is clearly observed in the spectra of P(6%)-CN, which is assigned to the P-N stretching mode. This is probably due to that the different phosphorus source causes the different P doping site.

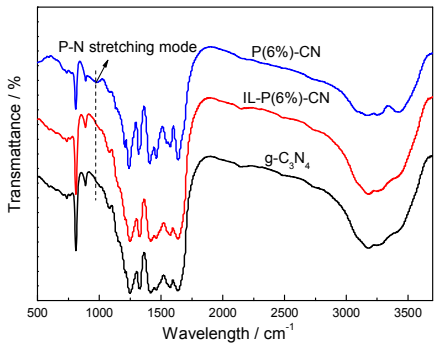


**Fig. 3** FT-IR spectra of synthesized g-$C_3N_4$, P(6%)-CN and IL-P(6%)-CN.

The light absorption property of as-prepared g-$C_3N_4$, P(x%)-CN and IL-P(6%)-CN catalysts is studied by UV-Vis spectra, and the results are shown in Fig. 4. Pure g-$C_3N_4$ shows a typical semiconductor absorption, originating from charge transfer response of g-$C_3N_4$ from the VB populated by N 2p orbitals to the CB formed by C 2p orbitals.[20] For P(x%)-CN, the obvious red shifts of absorption band were observed with increasing the phosphorus content, indicating phosphorus doping changed the optical property of synthesized g-$C_3N_4$, thus decreased the band gap energy. The band gap energy, which is calculated according to the method of Oregan and Gratzel, is 2.7 eV for g-$C_3N_4$. This is consistent with the previous results.[23-25] In the case of IL-P(6%)-CN, P(2%)-CN, P(4%)-CN, P(6%)-CN and P(10%)-CN, this value decreased to 2.68, 2.66, 2.65, 2.63 and 2.60 eV. This result is consistent with the academic calculation result of electronic structure of phosphorus doped g-$C_3N_4$ using first-principles reported by Ma et al.[26] They found a isolated P 3p state is localized just 0.15 eV below the bottom of the CB of the host g-$C_3N_4$, leading to the decreased band gap energy. For IL-P(6%)-CN, the absorption band was only slight changed compared with g-$C_3N_4$. This obvious difference in optical property between IL-P(6%)-CN and P(6%)-CN was probably due to the difference in P doping site. The possible reason is discussed (see below).

XPS were conducted to confirm the structure of g-$C_3N_4$ and the chemical state of phosphorus. In Fig. 5a and b, the spectra of g-$C_3N_4$ in both N 1s and C 1s region can be fitted with three contributions. For N 1s region (Fig. 5a), three contributions located at 398.2, 399.2 and 400.3 eV were assigned to the $sp^2$ hybridized aromatic nitrogen atoms bonded to carbon atoms (C-N=C), tertiary nitrogen N-$(C)_3$ groups linking structural motif or amino groups carrying hydrogen ($(C)_2$-N-H) inconnection with structural defects and incomplete condensation, and nitrogen atoms bonded three carbon atoms in the aromatic cycles.[27,28] In Fig. 5b, three components located at 284.6, 285.8 and 287.6 eV for g-$C_3N_4$ were attributed to the C-C bond which originated from $sp^2$ C atoms bonded to N in an aromatic ring (N-C=N), C=N or C≡N which could be ascribed to defect-containing $sp^2$ hybridized

carbon atoms present in graphitic domains and pure graphitic sites in a CN matrix.[29-31] It is shown in Fig. 5 that the spectra of P(6%)-CN and IL-P(6%)-CN in N 1s and C 1s regions also can be fitted with three contributions. However, the obvious shifts to higher binding energies were observed for P(6%)-CN and IL-P(6%)-CN in N 1s and C 1s regions compared with that of g-$C_3N_4$. This is probably due to the change of chemical environment after phosphorus doping. However, no obvious difference in binding energies between P(6%)-CN and IL-P(6%)-CN in N 1s and C 1s regions was observed, indicating the difference in P doping site did not influence the chemical environment of C and N atoms in g-$C_3N_4$.

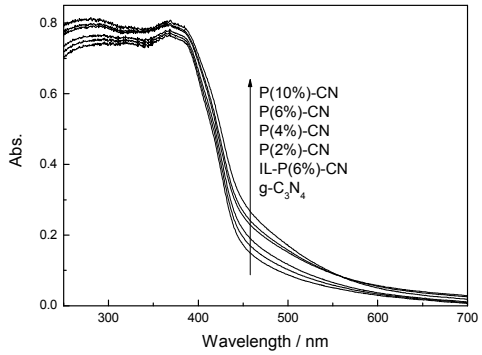


**Fig. 4** UV-Vis diffuse reflectance spectra of g-$C_3N_4$, P(x%)-CN and IL-P(6%)-CN.

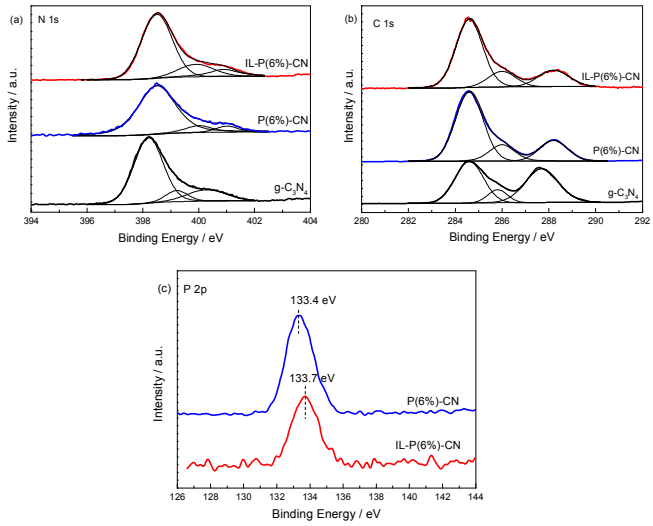


**Fig. 5** XP spectra of synthesized g-$C_3N_4$, P(6%)-CN and IL-P(6%)-CN in the region of N 1s (a), C 1s (b) and P 2p (c).

Fig. 5c showed that the binding energies of P(6%)-CN and IL-P(6%)-CN in P 2p region were located at 133.4 and 133.7 eV. It is reported that the binding energy of P 2p in P-N and P-C bonds was 133.5 eV and 131.5-132.5 eV, respectively.[14] Thus, it is deduced that phosphorus doped into g-$C_3N_4$ lattice in the formation of P-N bond. This binding energy difference, 0.3 eV, was probably due to the different chemical environment of P atoms in two catalysts. Zhang et al. suggested that the phosphorus heteratoms most probably replace the corner or bay carbon to form P-N bond in the doped $C_3N_4$ framework, as shown in Fig. 6a.[14] Ma et al. calculated the dopant formation energies and electronic properties of S and P doped g-$C_3N_4$ systems using first-principles density functional theory.[26] They suggested that S atom preferentially substitutes for the edge N atom of g-$C_3N_4$, whereas the P atom preferentially situates the interstitial sites of in-planar of g-$C_3N_4$, as shown in Fig. 6b. Obviously, in Fig. 6, P atoms bond to three N atoms when it replaces the carbon atoms. Whereas, only two P-N bonds formed when the interstitial doping occurs. Because the electronegativity of N atom is higher than that of P atom, more P-N bonds causes the lower electron density of P atoms, leading to the higher binding energy of IL-P(6%)-CN. Therefore, summarizes the obtained results above, it is deduced that P doping site is influenced by the phosphorus source. Substitutional doping occurs using [Bmim]$PF_6$ as phosphorus source, whereas interstitial doping occurs when $(NH_4)_2HPO_4$ is used. In addition, elemental analyse results revealed that the C/N ratio for g-$C_3N_4$ is 0.72, obviously higher than that of IL-P(6%)-CN (0.69). This is probably due to that partial C atoms were replaced by P atoms. However, for P(6%)-CN, this value is 0.71, similar to that of g-$C_3N_4$. This result confirms our point of view. Besides, the P concentrations in prepared catalysts were also measured by elemental analyse. The results indicated that the molar ratio of P element to g-$C_3N_4$ were 0.03, 0.056, 0.08, 0.11, 0.14 and 0.082 for P(2%)-CN, P(4%)-CN, P(6%)-CN, P(8%)-CN, P(10%)-CN and IL-P(6%)-CN. These values were very close to the theoretical value, indicating that P element did not lose during the preparation process.

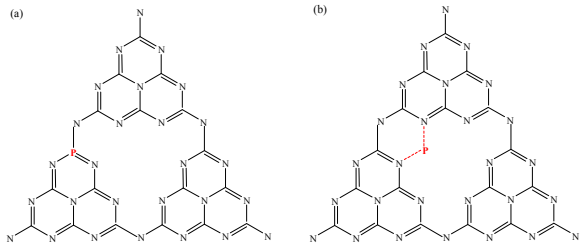


**Fig. 6** The possible doping sites of P atoms in g-$C_3N_4$.

Fig. 7 shows the room temperature PL spectra of g-$C_3N_4$, P(x%)-CN and IL-P(6%)-CN under the excitation wavelength of 320 nm. For g-$C_3N_4$, the broad PL band is around 465 nm, which can be attributed to the band-band PL phenomenon with the energy of light approximately equal to the band gap of g-$C_3N_4$ calculated by UV-Vis spectra.[30] Such band-band PL signal is attributed to excitonic PL, which mainly results from the n-π* electronic transitions involving lone pairs of nitrogen atoms in g-$C_3N_4$.[32] In the case of P doped g-$C_3N_4$, the shape of the curves is similar to that of g-$C_3N_4$, whereas the peak intensities significantly decrease. Considering that the PL emission results from the free charge carrier recombination, the decreased peak intensity indicates that P doped g-$C_3N_4$ exhibits lower electrons-holes recombination rate compared with g-$C_3N_4$. The previous calculation results show that phosphorus doping can increase the dispersion of the contour distribution of HOMO and LUMO, which improves the carrier mobility.[26] The noncoplanar HOMO

and LUMO favors the separation of photogenerated $e^-/h^+$ pairs and thus decreases the recombination rate. Obviously, the PL intensity of IL-P(6%)-CN is higher than that of P(6%)-CN. This indicated that P doping site could influence the separation rate of photogenerated $e^-/h^+$ pairs. Besides, the PL intensity of P(8%)-CN is stronger than that of P(6%)-CN, indicating the excess doping phosphorus could act as recombination centers for excited electrons and holes.

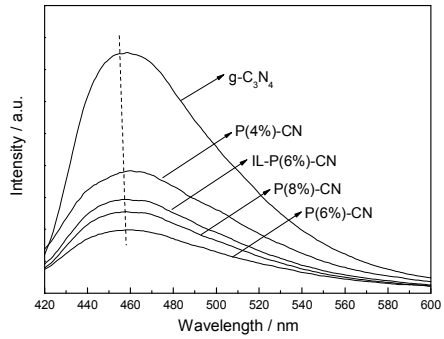


**Fig. 7** Photoluminescence emission spectra of g-$C_3N_4$, P(x%)-CN and IL-P(6%)-CN.

The generation of electrons-holes pairs as well as their separation, migration and capture by the reactive species is regarded as the basic process for the photocatalysis. Photoelectrochemistry test is a powerful tool to monitor these complicated processes. Fig. 8 shows the photocurrent responses of g-$C_3N_4$, P(6%)-CN and IL-P(6%)-CN. Obviously, the sharp increased photocurrent responses appeared for three catalysts once the pulse Xe lamp was applied. Besides, the photocurrent responses did not decay with increasing the illuminated time, indicating the prepared catalysts could provide stable quantity of electrons and holes during the irradiation. The photocurrent value of P(6%)-CN was much higher than that of g-$C_3N_4$ and IL-P(6%)-CN, which can be attributed to the more efficient separation of photogenerated electron-hole pairs.

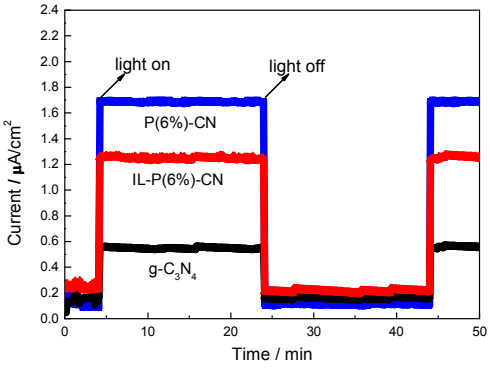


**Fig. 8** The photocurrent responses of g-$C_3N_4$, P(6%)-CN and IL-P(6%)-CN.

Fig. 9a shows the photocatalytic performances of g-$C_3N_4$, P(x%)-CN and IL-P(6%)-CN in the degradation of RhB under visible light irradiation. Before the light on, the RhB concentrations of P doped g-$C_3N_4$ were slightly lower than that of g-$C_3N_4$. This is probably due to that phosphorus doping changed the surface property of synthesized carbon nitride, leading to the improved RhB adsorption ability. Control experiments (not shown here) indicated that the RhB degradation rate can be ignored in the absence of either irradiation or photocatalyst, indicating that RhB was degraded via photocatalytic process. P(x%)-CN showed obviously higher activities than g-$C_3N_4$. The degradation rate increased with increasing x% to the maximum of 6%, beyond which the activity of the catalysts began to decrease. This trend is exactly opposite to the PL intensity order. Among the synthesized phosphorus doped g-$C_3N_4$ catalysts, no essential difference in optical property is shown in UV-Vis spectra, therefore the photocatalytic performance of P(x%)-CN is mainly determined by electrons-holes separation efficiency. When the P content was beyond the optimal value, the recombination of photogenerated electrons and holes increased, leading to the decreased activities of P(8%)-CN and P(10%)-CN. Besides, P(6%)-CN exhibited much higher activity than that of IL-P(6%)-CN. Considering that, the P concentration of P(6%)-CN and IL-P(6%)-CN which measured by elemental analyse is very close (molar ratio P/g-$C_3N_4$ = 0.08 and 0.082), the difference in photocatalytic performance between them should be not caused by the P concentration but by the different doping site. Interstitial P doping is more effective to improve the photocatalytic activity compared with substitutional P doping.

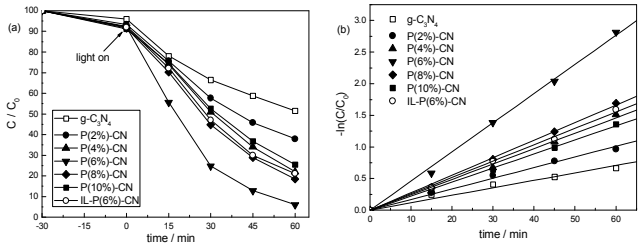


**Fig. 9** Photocatalytic performances of g-$C_3N_4$, P(x%)-CN and IL-P(6%)-CN (a) and plot of -ln($C/C_0$) against reaction time (b) in the degradation of RhB under visible light irradiation.

The reaction rate constant k was obtained by assuming that the reaction followed first order kinetics.[33] In a batch reactor, the performance equation is as follows: -ln($C/C_0$) = $kt$ where $C_0$ and $C$ represent the concentrations of RhB dye before and after photocatalytic degradation, respectively. If a linear relationship is established when -ln($C/C_0$) is plotted against $t$ (reaction time), the rate constant $k$ can be obtained from the slope of the line. Fig. 9b displays the plot of -ln($C/C_0$) against reaction time. The calculated results indicated that the rate constant $k$ was 0.0115, 0.0169, 0.0243, 0.0466, 0.0277, 0.0222 and 0.0258 $min^{-1}$ for g-$C_3N_4$, P(2%)-CN, P(4%)-CN, P(6%)-CN, P(8%)-CN, P(10%)-CN and IL-P(6%)-CN respectively. P(6%)-CN exhibited the highest rate constant which is 4 and 1.8 times higher than that of g-$C_3N_4$ and IL-P(6%)-CN. This increased photocatalytic performance should be attributed to the synergistic effect of decreased band gap energy which utilize visible light more efficiently, improved electrons-holes separation efficiency and increased RhB adsorption ability which caused by phosphorus doping.

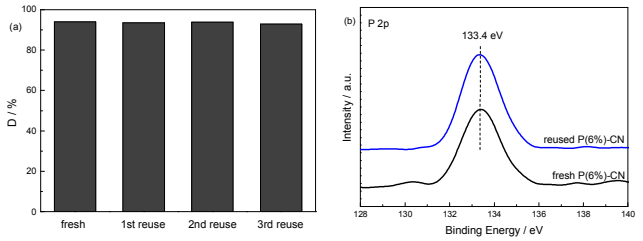


**Fig. 10** The catalytic stability test of P(6%)-CN (a) and comparison of XP spectra of fresh and reused P(6%)-CN in the region of P 2p (b).

To check the catalytic stability of P doped g-$C_3N_4$, the photocatalytic performance of P(6%)-CN was investigated in three circles (Fig. 10a). No obvious decrease in activity was observed after three circles, indicating that prepared P doped g-$C_3N_4$ is stable under visible-light irradiation. Moreover, the P element concentrations of fresh and reused P(6%)-CN which measured by elemental analyse were 0.08 and 0.081. No essential difference was observed between them, indicating the structure of P(6%)-CN is stable. Fig. 10b shows the comparison of XP spectra of fresh and reused P(6%)-CN in the region of P 2p. The binding energy is not changed after three circles, indicating that the chemical state of P element is stable.

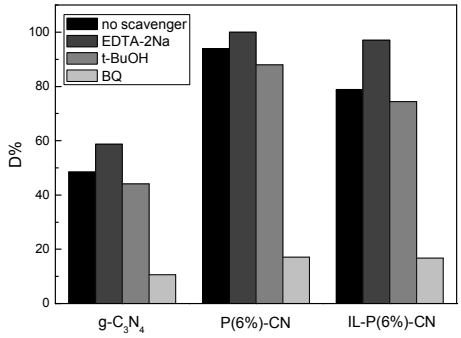


**Fig. 11** Influence of various scavengers on the visible light photocatalytic activity of g-$C_3N_4$, P(6%)-CN and IL-P(6%)-CN.

In order to clarify the mechanism on the improved activity of phosphorus doped g-$C_3N_4$ in depth, the active species generated during the reaction process are identified by hole and free radical trapping experiment. In this investigation, EDTA-2Na, tert-butyl alcohol (t-BuOH) and 1,4-benzoquinone (BQ) are used as the hole ($h^+$) scavenger, hydroxyl radical (•OH) scavenger and superoxide radical ($•O^{2-}$) scavenger, respectively.[34] Fig. 11 shows the influence of various scavengers on the visible light photocatalytic activity of g-$C_3N_4$, P(6%)-CN and IL-P(6%)-CN. For g-$C_3N_4$, the photodegradation rate of RhB decreased slightly after the addition of t-BuOH, indicating that hydroxyl radicals are not the main active species in current photocatalytic systems. When BQ was added, the degradation of RhB was inhibited sharply, indicating $•O_2^-$ is the main active species in current photocatalytic systems. It is reported that the CB and VB of g-$C_3N_4$ were -1.12 V and +1.57 V, respectively.[21] Whereas, the redox potentials for $•OH/OH^-$ and $O_2/•O_2^-$ were determined to be +1.99 V and -0.33 V.[35] Therefore, the reduction potential of CB electrons in g-$C_3N_4$ was negative enough to reduce $O_2$ to form $•O_2^-$, whereas the VB holes in g-$C_3N_4$ were not positive enough to generate •OH. This is consistent with our experiment results. In the presence of EDTA-2Na, the RhB degradation rate is increased obviously, which is different from previous result.[34] Zhang et al. prepared $C_3N_4/Bi_5Nb_3O_{15}$ heterojunction catalyst for 4-CP photodegradation.[34] The photodegradation rate was decelerated significantly after the addition of EDTA-2Na, indicating the direct photogenerated holes oxidation happened. In our investigation, although the redox potential of RhB is reported to be 1.43 V,[36] which is higher than the VB of g-$C_3N_4$, the direct photogenerated holes oxidation did not happen. On the contrary, the addition of EDTA-2Na to trap the $h^+$ can promote the separation rate of $e^-/h^+$ pairs, leading to the increased photocatalytic performance. For P(6%)-CN and IL-P(6%)-CN, the similar trend was obtained, indicating the main oxidative species is the same as that of g-$C_3N_4$. The difference in phosphorus doping site does not change the reaction mechanism.

## Conclusions

Phosphorus doped g-$C_3N_4$ was prepared conveniently by a simple method using dicyandiamide monomer and diammonium hydrogen phosphate as precursors. The introduction of phosphorus inhibited the crystal growth of graphitic carbon nitride, decreased the band gap energy and increased the separation efficiency of photogenerated electrons and holes. Phosphorus atoms doped into g-$C_3N_4$ lattice in the formation of P-N bond. P doping site is influenced by the phosphorus source. Substitutional doping occurs using $[Bmim]PF_6$ as phosphorus source, whereas interstitial doping occurs when $(NH_4)_2HPO_4$ is used. The results of photocatalytic RhB degradation indicated that the rate constant of P(6%)-CN was 0.0466 $min^{-1}$, which is 4 and 1.8 times higher than that of g-$C_3N_4$ and IL-P(6%)-CN. Moreover, P(6%)-CN exhibited stable catalytic activity and chemical structure. Interstitial P doping is more effective to improve the photocatalytic activity compared with substitutional P doping. The superoxide radical $•O_2^-$ is the main active species for RhB degradation in both P(6%)-CN and g-$C_3N_4$ systems. The difference in phosphorus doping site does not change the reaction mechanism.

## Acknowledgment

This work was supported by Program for New Century Excellent Talents in University (No. NCET-11-1011), National Natural Science Foundation of China (No. 41071317, 30972418, 21103077), National Key Technology R & D Programme of China (No. 2007BAC16B07, 2012ZX07505-001), the Natural Science Foundation of Liaoning Province (No. 20092080), and the Natural Science Foundation of Liaoning Shihua University (No. 2011XJJ-021).

## Notes and references

[a] *Institute of Eco-environmental Sciences, Liaoning Shihua University, Fushun 113001, PR China. E-mail: hushaozhenglnpu@163.com; Tel: 86-24-56860865*

[b] School of Petrochemical Engineering, Liaoning Shihua University, Fushun 113001, P.R. China
[c] School of Environmental and Biological Engineering, Liaoning Shihua University, Fushun 113001, PR China
[d] College of Chemistry and Materials Science, Liaoning Shihua University, Fushun 113001, PR China

1 M.R. Hoffmann, S.T. Martin, W. Choi and D.W. Bahnemann, *Chem. Rev.,* 1995, **95**, 69-96.
2 A. Fujishima, T.N. Rao and D.A. Tryk, *J. Photochem. Photobiol. C,* 2000, **1**, 1-21.
3 R. Asahi, T. Morikawa, T. Ohwaki, A. Aoki and Y. Taga, *Science,* 2001, **293**, 269-271.
4 P.D. Cozzoli, R. Comparelli, E. Fanizza, M.L. Curri, A. Agostiano and D. Laub, *J. Am. Chem. Soc.,* 2004, **126**, 3868-3879.
5 X. Zong, H.J. Yan, G.P. Wu, G.J. Ma, F.Y. Wen, L. Wang and C. Li, *J. Am. Chem. Soc.,* 2008, 1**30**, 7176-7177.
6 W.Q. Fan, Q.H. Lai, Q.H. Zhang and Y. Wang, *J. Phys. Chem. C,* 2011, **115**, 10694-10701.
7 B. Zielinska, E. Borowiak-Palen and R.J. Kalenczuk., *Int. J. Hydrogen Energy,* 2008, **33**, 1797-1802.
8 A. Tanaka, S. Sakaguchi, K. Hashimoto and H. Kominami, *ACS Catal.,* 2013, **3**, 79-85.
9 K. Li, B. Chai, T.Y. Peng, J. Mao and L. Zan, *ACS Catal.,* 2013, **3**, 170-177.
10 X.F. Chen, X.C. Wang, Y.D. Hou, J.H. Huang, L. Wu and X.Z. Fu, *J. Catal.,* 2008, **255**, 59-67.
11 S.Z. Hu, F.Y. Li and Z.P. Fan, *J. Hazard. Mater.,* 2011, **196**, 248-254.
12 S.C. Yan, Z.S. Li and Z.G. Zou, *Langmuir,* 2009, **25**, 10397-10401.
13 J.S. Zhang, M.W. Zhang, G.G. Zhang and X.C. Wang, *ACS Catal.,* 2012, **2**, 940-948.
14 Y.J. Zhang, T. Mori, J.H. Ye and M. Antonietti, *J. Am. Chem. Soc.,* 2010, **132**, 6294-6295.
15 L.G. Zhang, X.F. Chen, J. Guan, Y.J. Jiang, T.G. Hou and X.D. Mu, *Mater. Res. Bull.,* 2013, **48**, 3485-3491.
16 X.J. Bai, R.L. Zong, C.X. Li, D. Liu, Y.F. Liu and Y.F. Zhu, *Appl. Catal. B: Environ.,* 2014, **147**, 82-91.
17 X.F. Chen, J.S. Zhang, X.Z. Fu, M. Antonietti and X.C. Wang, *J. Am. Chem. Soc.,* 2009, **131**, 11658-11659.
18 Y. Wang, J.S. Zhang, X.C. Wang, M. Antonietti and H.R. Li, *Angew. Chem. Int. Ed.,* 2010, **49**, 3356-3359.
19 J. Ma, S. Li and Y. Jiang, *Macromolecules,* 2002, **35**, 1109-1115.
20 X.C. Wang, K. Maeda, A. Thomas, K. Takanabe, G. Xin, K. Domen and M. Antonietti, *Nat. Mater.,* 2009, **8**, 76-80.
21 Y. Wang, X.C. Wang and M. Antonietti, *Angew. Chem. Int. Ed.,* 2012, **51**, 68-89.
22 Y.Y. Bu, Z.Y. Chen and W.B. Li, *Appl. Catal. B: Environ.,* 2014, **144**, 622-630.
23 H.J. Yan and H.X. Yang, *J. Alloys Comp.,* 2011,**509**, L26-L29.
24 B. Oregan and M. Gratzel, *Nature,* 1991, **353**, 737-740.
25 X.C. Wang, S. Blechert and M. Antonietti, *ACS Catal.,* 2012, **2**, 1596-1606.
26 X.G. Ma, Y.H. Lv, J. Xu, Y.F. Liu, R.Q. Zhang and Y.F. Zhu, *J. Phys. Chem. C,* 2012, **116**, 23485-23493.
27 Z.X. Ding, X.F. Chen, M. Antonietti and X.C. Wang, *Chemsuschem,* 2011, **4**, 274-281.
28 Y.W. Zhang, J.H. Liu, G. Wu and W. Chen, *Nanoscale,* 2012, **4**, 5300-5303.
29 B. Chai, T.Y. Peng, J. Mao, K. Li and L. Zan, *Phys. Chem. Chem. Phys.,* 2012, **14**, 16745-16752.
30 L. Ge and C. Han, *Appl. Catal. B: Environ.,* 117/118 (2012) 268-274.
31 W. Lei, D. Portehault, R. Dimova and M. Antoniettit, *J. Am. Chem. Soc.,* 2011, **133**, 7121-7127.
32 V.N. Khabashesku, J.L. Zimmerman and J.L. Margrave, *Chem. Mater.,* 2000, **12**, 3264-3270.
33 X.Y. Li, D.S. Wang, G.X. Cheng, Q.Z. Luo, J. An and Y.H. Wang, *Appl. Catal. B: Environ.,* 2008, **81**, 267-273.
34 S.Q. Zhang, Y.X. Yang, Y.N. Guo, W. Guo, M. Wang,Y.H. Guo and M.X. Huo, *J. Hazard. Mater.,* 2013, **261**, 235-245.
35 G. Liu, P. Niu, L.C. Yin and H.M. Cheng, *J. Am. Chem. Soc.,* 2012, **134**, 9070-9073.
36 T. Shen, Z.G. Zhao, Q. Yu and H.J. Xu, *J. Photochem. Photobiol. A: Chem.,* 1989, **47**, 203-212.